

FULL PAPER

Open Access



Various far-field hydrological responses during 2015 Gorkha earthquake at two distant wells

Xudong Huang¹ and Yu Zhang^{1,2*} 

Abstract

Aquifer hydraulic parameter can change during earthquakes. Continuous monitoring of the response of water level to seismic waves or solid Earth tides provides an opportunity to document how earthquakes influence hydrological properties. Here, we use data of two groundwater wells, Dian-22 (D22) and Lijiang (LJ) well, in southeast Tibet Plateau in response to the 2015 Mw 7.8 Gorkha earthquake to illustrate hydrological implications. The coherences of water level and seismic wave before and after the far-field earthquake show systematic variations, which may confirm the coseismic dynamic shaking influence at high frequencies ($f > 8$ cpd). The tidal response of water levels in these wells shows abrupt coseismic changes of both phase shift and amplitude ratio after the earthquake, which may be interpreted as an occurrence in the vertical permeability of a switched semiconfined aquifer in the D22 well, or an enhancement unconfined aquifer in the LJ well. Using the continuous short-term transmissivity monitoring, we show that the possible coseismic response for about 10 days and instant healing after 10 days to the causal earthquake impact. Thus, the dynamic shaking during the Gorkha earthquake may have caused the short-term aquifer responses by reopening of preexisting vertical fractures and later healing at epicentral distances about 1500 km.

Keywords: Earthquake, Water level, Coherence, Tidal response, Transmissivity

Introduction

It has been widely reported that earthquakes can cause various hydrological responses, such as changes in groundwater level (Roeloffs 1998; Brodsky et al. 2003), increases in stream flow (Muir-Wood and King 1993; Manga, 2001; Wang et al. 2004a; Wang and Manga 2015), water-temperature variations (Mogi et al. 1989; Shi et al. 2007; Wang et al. 2013; Shi and Wang 2014; Zeng et al. 2015; Ma 2016) and chemical composition release (Claesson et al. 2004; Skelton et al. 2014; Zeng et al. 2015), which are always interpreted by induced underground water transport (e.g., Claesson et al. 2007; Wang et al. 2013). Different mechanisms have been

proposed to explain these coseismic transport enhancement phenomena, including changes in aquifer permeability or storativity (Rojstaczer et al. 1995; Wang et al. 2004a; Manga et al. 2012; Zhang et al. 2019a, b), static stress and dynamic stress induced pore pressure diffusion (Muir-Wood and King 1993; Jónsson et al. 2003), consolidation/liquefaction of saturated sediments (Manga 2001; Manga et al. 2003), rupturing and unclogging of fractures (Sibson and Rowland 2003; Wang et al. 2004b), and water recharging tank (Kagabua et al. 2020). In phenomenological analysis of this underground flow, the coseismic change in permeability always can be adopted, which also usually attaches to horizontal flow in observation wells (Elkhoury et al. 2006; Xue et al. 2013; Shi et al. 2015) since permeability of a layered groundwater system in the horizontal direction is normally larger than that in the vertical direction (Liao et al. 2015). Recent studies show that near

*Correspondence: yuz124@gmail.com; yuzhang@sgg.whu.edu.cn

¹ School of Geodesy and Geomatics, Wuhan University, Wuhan 430079, China

Full list of author information is available at the end of the article

field and intermediate earthquakes may also breach the aquitards between aquifers and increase vertical permeability (Wang et al. 2004a, 2018; Shi and Wang 2014, 2016; Zhang et al. 2019a, b) that can explain some unexpected aquifer hydrological responses at near field.

Groundwater level monitoring plays an important part in the earthquake prediction program in China, and a nationwide groundwater monitoring well network has been constructed for this purpose (Shi et al. 2015). In this work, we examine the water-level responses at the Dian-22 (D22) and Lijiang (LJ) wells at southeast margin of Tibet Plateau due to the 2015 Mw 7.8 Nepal Gorkha earthquake (Fig. 1). The distant earthquake (> 1000 km) induced distinct coseismic water-level responses in these two adjacent wells at successive days. The D22 well may be caused by a switched coseismic vertical diffusion, while the LJ well may be caused by a coseismic enhancement in vertical aquifer leakage. It indicates the seismic wave may induce vertical groundwater flow in this far field. We try to interpret the earthquake-induced changes using moving time-window coherence with regards to seismic and atmospheric excitations to identify the time-dependent hydrological responses in preseismic, coseismic and postseismic phases. Thus, the tidal responses of groundwater in these wells are further interpreted by the transmissivity variations by continuous tidal analysis using different ground flow models. Furthermore, we infer that the preexisting fractures unclogging

and reclogging by seismic shaking during the earthquake and the local site amplification may favor this effect on shallow hydrological systems at epicentral distances > 1000 km.

Observations and data

The April 2015 Nepal Gorkha earthquake occurred at Main Himalayan thrust (MHT) for ~140 km east–west and ~50 km across strike and 80 km WNW of Kathmandu, with a hypocentral depth of ~15 km. The focal mechanism indicated thrusting on a sub-horizontal fault dipping at ~10° north, which nucleated approximating to the brittle–ductile transition and propagated east along the MHT but did not rupture to the surface (see Fig. 1; Avouac et al. 2015; Elliott et al. 2016).

We have collected the water-level data from two distant wells with distinct coseismic responses to the earthquake located in the south boundary of the Tibet Plateau (also see Fig. 1). The D22 well is located near the center of Luxi Basin. According to drilling data, the well with 200.17 m depth is cased with pipe to 95.57 m, with a screened interval between 95.57 and 200.17 m. It is drilled with a diameter of 168 mm to 6.1 m, and with a diameter of 146 mm from 6.1 and 56.84 m. The diameter between 56.84 and 95.57 m is 127 mm, and at much deeper levels the well has no casing (see details in Fig. 2a and Table 1). The LJ well is situated at the north end of Honghe (HH) fault zone, at the intersection of Lijiang–Jianchuan (LJ–JS) fault and Zhongdian–Dali (ZD–DL) fault (Feng et al. 2004). The well is drilled to 310 m and cased with pipe to 240 m, with a screened interval between 240 and 310 m. Within 20 m depth, the well diameter is 194 mm. And the diameter reduces to 166 mm to the depth of 80 m. At depth of 80–240 m the well diameter is 127 mm. The rest part of the well has the diameter of 108 mm (see details in Fig. 2b and Table 1).

The water level is measured by an LN-3A digital water-level gauge (Institute of Seismic Science, China Earthquake Administration). It converts the reading of the digital pressure measurement into the groundwater level. The sampling is 1 min with the resolution of 1 mm, and the absolute accuracy is 0.2%. The along well seismic waves are recorded by the CTS-1 broad-band seismometer with sampling of 0.01 s. Seismic-wave and water-level data collected from February 8 to August 7 2015 are analyzed.

Coseismic response identifications

Preseismic, coseismic and postseismic water-level changes caused by the Gorkha earthquake are clearly identified in the seismic wave and water-level data (Figs. 3 and 4). Compared with the long-term water-level oscillation, the water-level show obvious coseismic

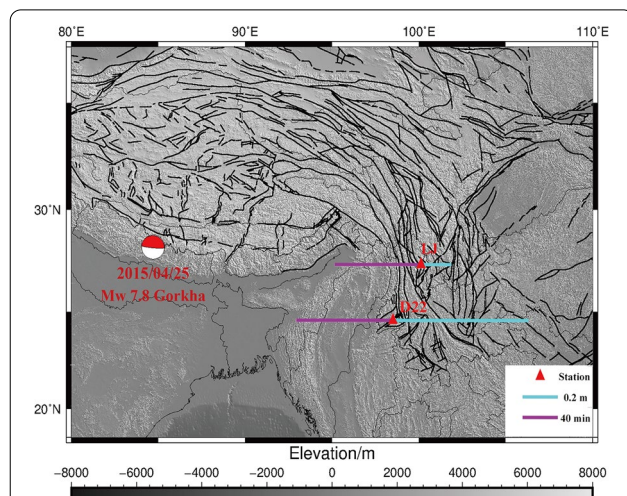


Fig. 1 Map showing the locations of the D22 well and LJ well (red solid triangles). 'Beach ball' shows the epicenter and focal mechanism of the 2015 Mw 7.8 Gorkha earthquake (Avouac et al. 2015). Black lines denote the location of surface faults on the Chinese mainland (Deng et al. 2006). The blue and purple lines indicate the variation amplitude and duration of water-level responses to The Gorkha earthquake, respectively

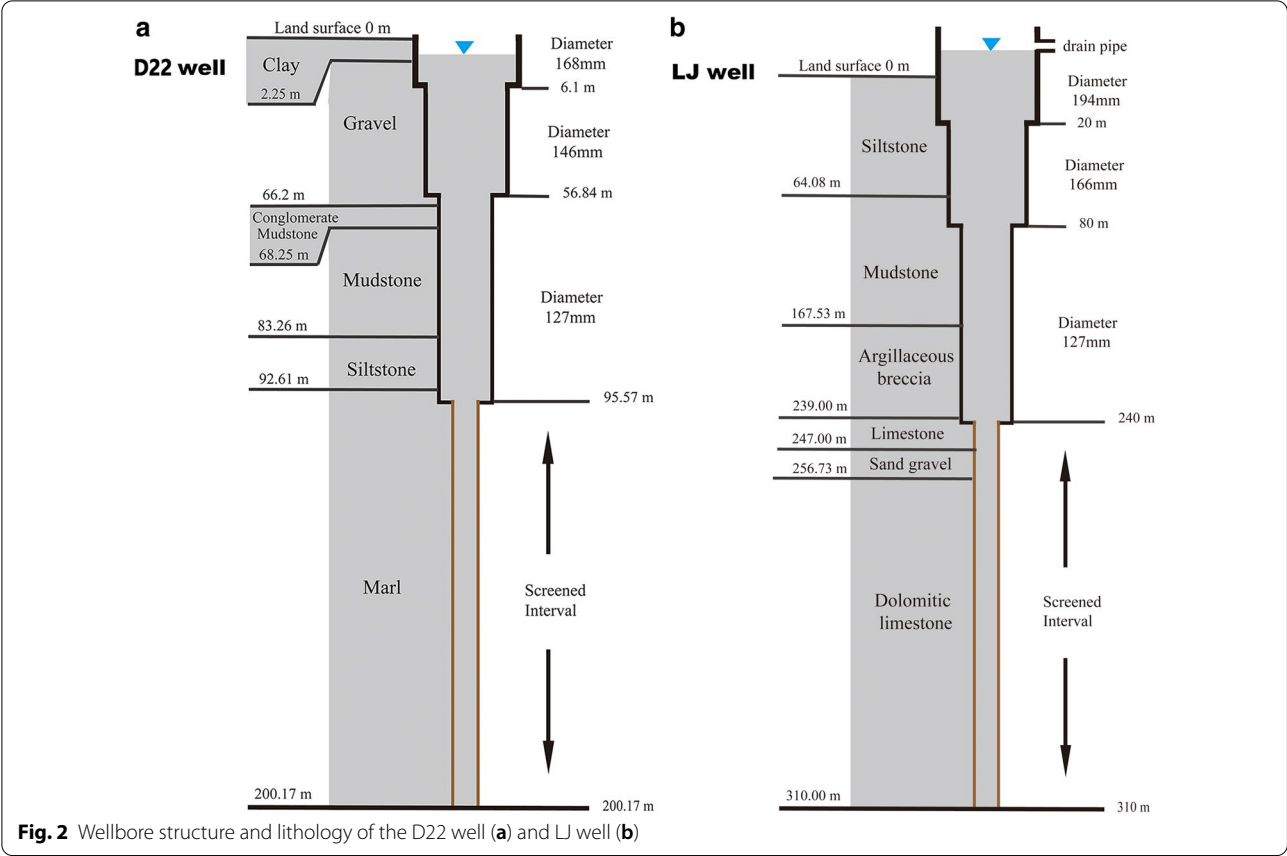


Fig. 2 Wellbore structure and lithology of the D22 well (a) and LJ well (b)

Table 1 Observation wells to Gorkha earthquake

Station	Lat (°)	Lon (°)	Ele (m)	EP (km)	Aquifer Lithology	Depth (m)	WL (m)
D22	98.6	24.2	924	1445.4	marl	200.17	0.76
LJ	100.2	26.9	2428	1530.9	limestone	310.00	0.16

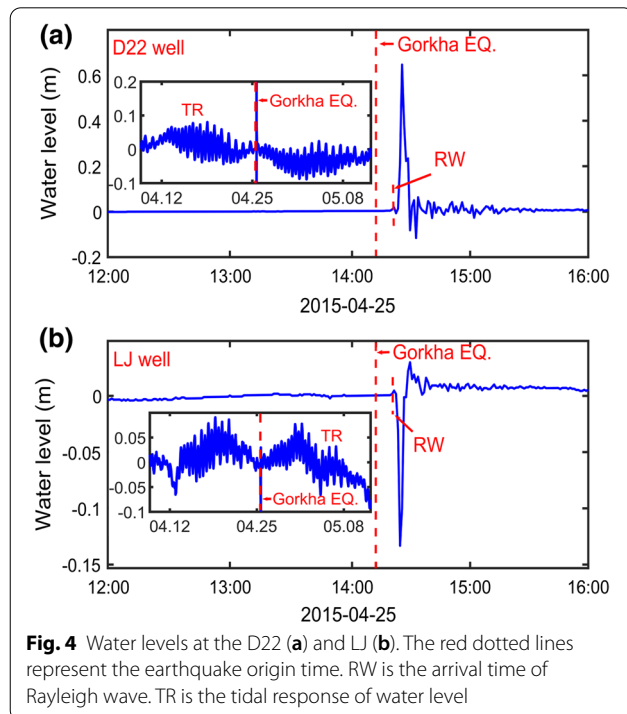
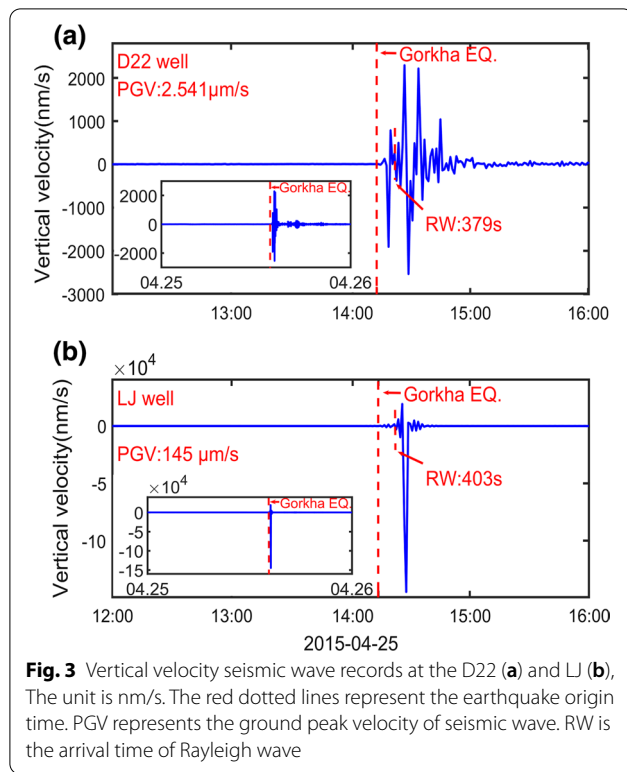
EP is the epicenter distance, WL stands for the maximum coseismic water-level variation

impulses with short-term sustained postseismic variation mentioned as the duration times (see Fig. 1). The approximate durations of the short-term coseismic water level sustainable changes (the recovery times) are also measured by when the water level decreases down to 5% of the maximum coseismic response with the tidal response removal. The amplitudes of the coseismic water-level changes are also shown in Table 1 and Fig. 1. We calculate the difference between the levels within 2 h after the origin time of the Gorkha earthquake to get the amplitude of the oscillation in each well (Ma and Huang, 2017). On comparing the seismic wave (Fig. 3) with the water level (Fig. 4), it is easy to distinguish the coseismic water-level response to the Gorkha earthquake in the D22 well and LJ well whose maximum amplitudes of 0.76 m and

0.16 m, respectively. The duration times of the coseismic water-level changes are 109 min and 97 min. By exact checking of the seismic-wave and water-level time windows, we can discover that the coseismic water-level response mainly corresponds to the Rayleigh surface-wave arrival times (see Figs. 3 and 4). These results suggest that the oscillation amplitudes and afterward durations of the coseismic water-level changes are associated with teleseismic surface-wave oscillations.

Coseismic coherency analysis

To estimate how the seismic wave influences the water level, we first calculated the cross ordinary coherence functions γ_{xy}^2 among the water level, vertical velocity seismograms and barometric pressure for each station (Lai



et al. 2013). The ordinary coherence function is defined as

$$\gamma_{xy}^2 = \frac{|G_{xy}(\omega)|^2}{G_{xx}(\omega)G_{yy}(\omega)}, \quad (1)$$

where $G_{xx}(\omega)$ and $G_{yy}(\omega)$ are the power spectra of two signals, respectively, and $G_{xy}(\omega)$ is the cross-power spectrum between them.

In the calculation, we use the data of each 3 days around the earthquake from April 23, 2015 to April 28, 2015. These data are continuous and stable. The time window and overlap are 1024 min and 512 min, respectively. We calculate the coherence before, around and after the earthquake origin time (Figs. 5 and 6). Previous studies show that the barometric pressure and Earth tide are two persistent factors affecting the water-level change (e.g., Lai et al. 2013; Zhang et al. 2019a, b). Because barometric pressure is one of the factors of well water-level change, the coseismic influence of seismic wave on water level in a well may be contaminated by it. We must exclude the possibility that barometric pressure has influence on the seismic wave, and determine the potential coseismic relationship between seismic wave and water level. The great transfer efficiency of semidiurnal tide for water level locates around 1–8 cpd. In the low-frequency band ($f < 1$ cpd), the barometric pressure also shows the great transfer efficiency for most wells whose ordinary coherence functions are up to 0.9. In the high-frequency band ($f > 8$ cpd), both efficiencies for water level decrease though (Lai et al. 2013). However, in the D22 well, we can observe the high efficiencies from barometric pressure, which may be caused by the in-well barometer. The coseismic shaking breaks this high coherence in this high-frequency band (Fig. 5c second panel), while the water-level response to velocity show the coherence enhancement between the preseismic and postseismic stages (see Figs. 5a, second panel). At the postseismic stage, the low-frequency ($f < 8$ cpd) transfer efficiencies of velocity from water level and barometric pressure increases (up to 0.7) in semidiurnal tide band which may represent in-phase responses of the semidiurnal tides and post seismic hydrological recovery. The coseismic coherence of barometric pressure and vertical velocity shows little downward at high frequencies. In the low-frequency band, the increased coherence may represent the tide transfer efficiencies in the both time series. In the LJ well, we can observe the similar water level in response to the velocity excited by the seismic waves at different stages (Fig. 6a). The barometric pressure transfer efficiencies to water level do not show obvious coseismic change as mainly affected in the 1–8 cpd (Fig. 6c), as previous mentioned (Lai et al. 2013). It is noted that the coherence

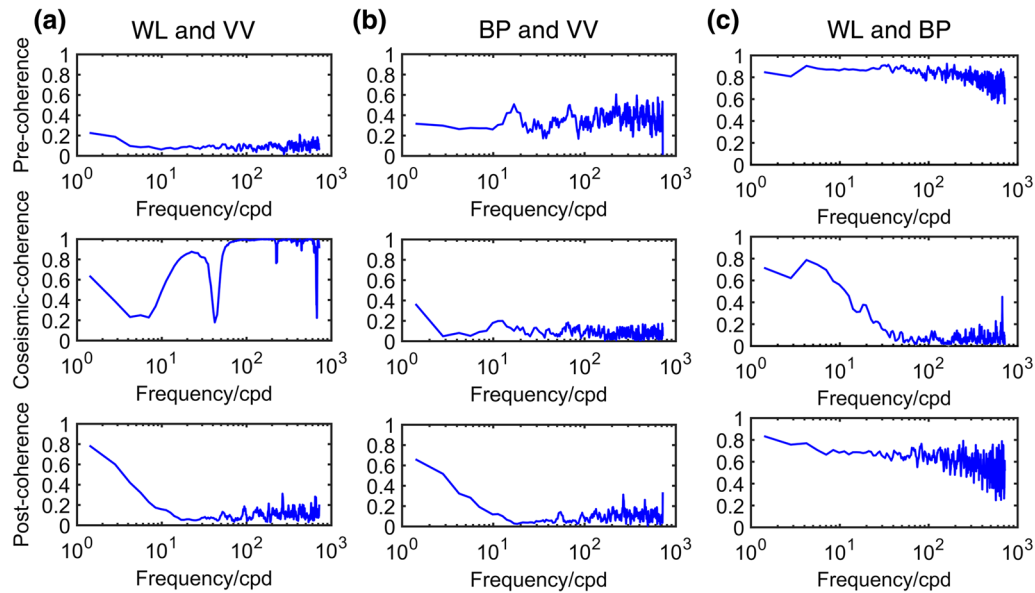


Fig. 5 Gorkha earthquake preseismic, coseismic and postseismic coherences between water level and vertical velocity (a), barometric pressure and vertical velocity (b), as well as water level and barometric pressure (c) in the D22 well. WL, VV and BP are abbreviations of water level, coseismic and barometric pressure, respectively. Figure 6 Gorkha earthquake preseismic, coseismic and postseismic coherences between water level and vertical velocity (a), barometric pressure and vertical velocity (b), as well as water level and barometric pressure (c) in the LJ well. WL, VV and BP are abbreviations of water level, coseismic and barometric pressure, respectively

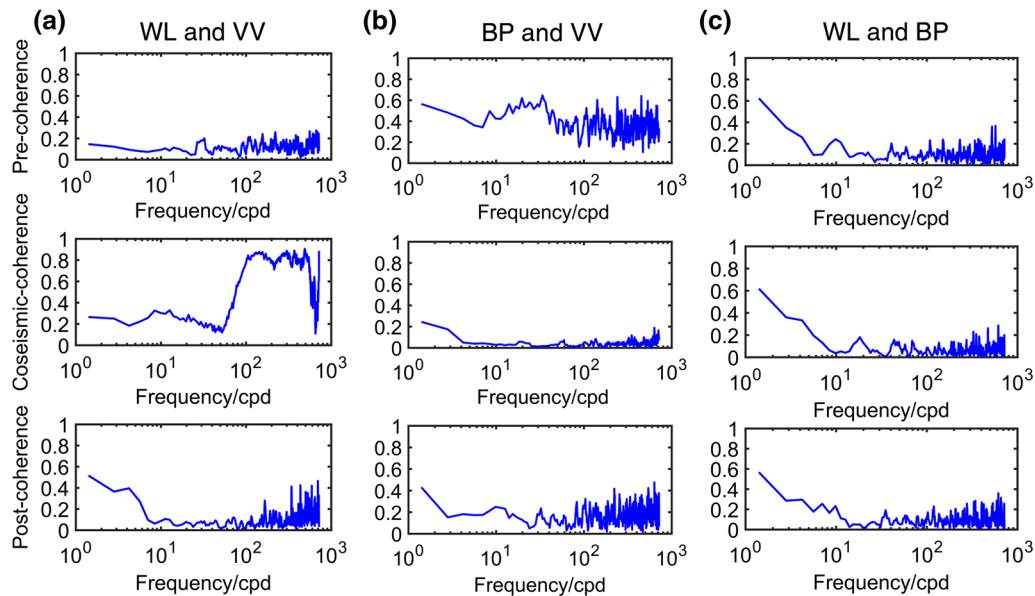


Fig. 6 Gorkha earthquake preseismic, coseismic and postseismic coherences between water level and vertical velocity (a), barometric pressure and vertical velocity (b), as well as water level and barometric pressure (c) in the LJ well. WL, VV and BP are abbreviations of water level, coseismic and barometric pressure, respectively

between the velocity and barometric pressure show the similar coseismic decrease in the high-frequency band ($f > 8$ cpd) as that between the water level and barometric

pressure in the D22 well (comparing Figs. 5c and 6b). An open well barometric pressure and seismic wave observation may make this correspondence. The relative high

coherence except the coseismic stage may come from the wind noise. In short, the Gorkha earthquake coseismic responses directly may shake in high-frequency band ($f > 8$ cpd), and further switched the low-frequency semi-diurnal tide transfer efficiencies (1–8 cpd), which further illustrate far field the hydrological responses to the great earthquake.

Aquifer tidal response analysis

Among the tidal constituents, the O1 and M2 tides have large amplitudes and with low barometric effect. Therefore, they are the constituents most widely used in tidal analysis (e.g., Zhang et al. 2016; Wang et al. 2019). The M2 tide is more popular for its higher accuracy at 12.42 h period (Hsieh et al. 1987; Rojstaczer and Agnew 1989; Doan et al. 2006), which we apply for the following tide analysis.

The amplitude and phase responses of water level to the M2 tide can reflect aquifer storativity and permeability around well (Hsieh et al. 1987; Elkhoury et al. 2006; Doan et al. 2006; Xue et al. 2013). In a confined system, high permeability usually causes small phase lags, whereas low permeability results in large phase lags. The amplitude response is primary to measure specific storage (Zhang et al. 2016).

According to Cooper et al. (1965), the steady fluctuation of water level in a well occurs at the same frequency as the harmonic pressure head disturbance in the aquifer which, however, leads to different amplitude and phase shift. Hsieh et al. (1987) described the pressure head disturbance and water-level response as

$$h_f = h_0 \exp(i\omega t), \quad (2)$$

$$x = x_0 \exp(i\omega t), \quad (3)$$

where h_f denotes the fluctuating pressure head in the aquifer. h_0 is the complex amplitude of the pressure head fluctuation. x is the water level from the static position. x_0 is the complex amplitude of the water-level fluctuation. t indicates the time. $\omega = 2\pi/\tau$ is the frequency of fluctuation, where τ is the period of fluctuation. The ratio between the amplitude of the water-level and that of the pressure head defines the amplitude response A as

$$A = |x_0/h_0|. \quad (4)$$

The phase shift is defined as

$$\eta = \arg(x_0/h_0), \quad (5)$$

where $\arg()$ is the argument of a complex number.

Figures 7 and 8 show the M2 tidal wave amplitude and phase response of water level in the D22 and LJ well, respectively. The blue error bars indicate the

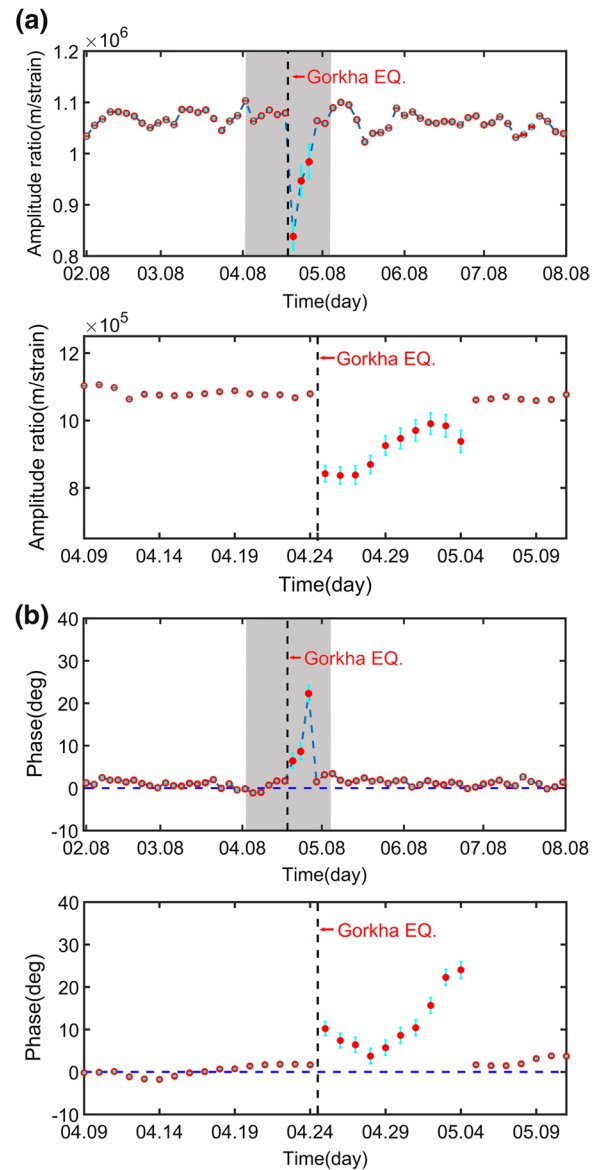


Fig. 7 Amplitude ratio (a) and phase response (b) of D22 well at M2 wave frequency change with time. Amplitude response is amplitude ratio of earth tide and water level. Dotted line shows the origin time of 2015 Gorkha earthquake (Beijing time). Blue error bars indicate the error of the tidal analysis. Bottom panels in figures a and b are the magnifications of the corresponding period of the gray background in the top panels, respectively

root-mean-square error (RMSE) of the tidal analysis. The bottom panels in figures (a) and (b) are the magnifications of the corresponding period of the gray background in the top panels, respectively. The M2 tidal signal is decomposed using the Baytap-G software based on Bayesian statistics (Tamura et al. 1991). Steps and spikes caused by instrument malfunctions or maintenance work

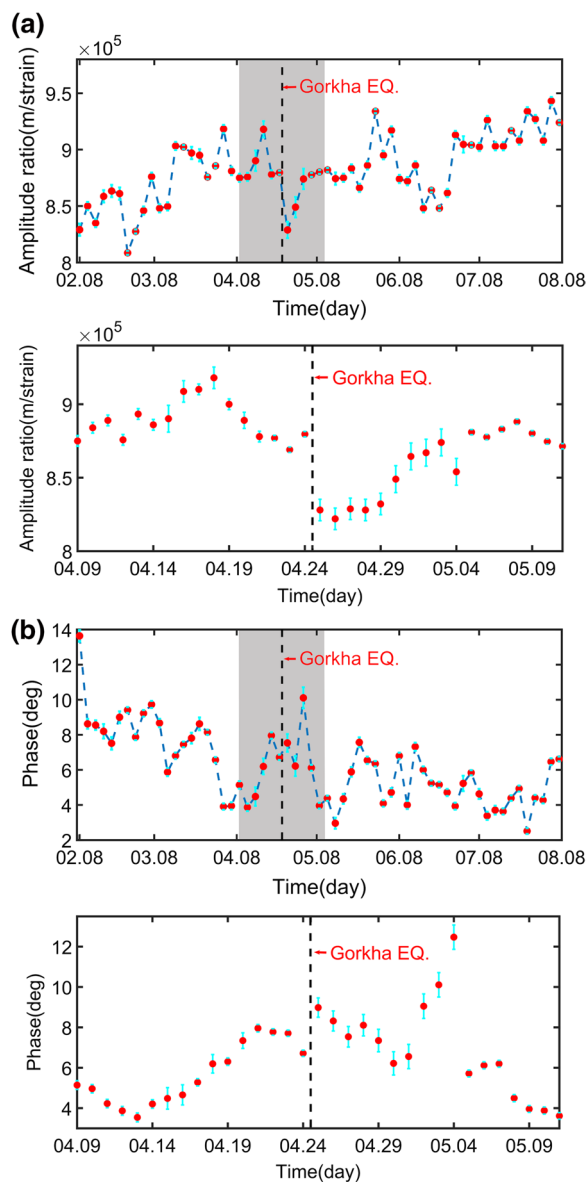


Fig. 8 Amplitude ratio (a) and phase response (b) of LJ well change with time at M2 wave frequency. Amplitude response is amplitude ratio of earth tide and water level. Dotted line shows the origin time of 2015 Gorkha earthquake (Beijing time). Blue error bars indicate the error of the tidal analysis. Bottom panels in figures a and b are the magnifications of the corresponding period of the gray background in the top panels, respectively

are removed before the analysis. The barometric correction is performed by local barometric data. We use the data from February 8 to August 7 in 2015 when there were no other large earthquakes. The 10-day time window is selected to determine the amplitude and phase responses, since Elkhoury et al. (2006) have proven that using 240-h or 10-day time window can differentiate the

M2 and S2 tidal constituents sufficiently. We have applied the Baytap-G software with different time windows to two different synthetic datasets (see Additional file 1: Text S1–S2 in the support information). The phase-shift estimations have proven that a 10-day time window is sufficient to separate the M2 and S2 tides and detect the phase changes (see Additional file 1: Figures S1–S4). Previous study (Shi et al. 2013) and our test may validate that the Baytap-G software with this fine time window selection can be applied appropriately for the M2 tide analysis. In our data processing, the time label for each time window is the last day of the 10 days for the causal signal of the coseismic hydrological response which the past influences the present (Menke and Menke 2016). We thought in this way the coseismic changes can be reflected causally in time. Otherwise, there may be a delay for the standardization of coseismic variations in this small time-step analysis. We find during the coseismic days, the responses show significant variations that break the background long-term seasonal trend. The transient amplitude ratio decrease and the transient phase-shift increase in both wells caused by the Gorkha earthquake in two wells can be clearly distinguished and identified, which are consistent to the time-dependent coherence analysis. Near zero phase before the earthquake becomes positive after the earthquake for the D22 well (from 0° to 10°). While the positive phase before the earthquake becomes larger after the earthquake for the LJ well (from 7° to 9°), and restores at the postseismic phase. When the day of the coseismic well water-level response appears into the end of the time window, the changes of the response show in the fitting for amplitude and phase shift. The larger variations of amplitude ratio, and phase shift appears when the successive days after the earthquake go into the time window. But, we also find when the coseismic day moves out the beginning of the time window, the tidal response damps as the ordinary time. A complete successive causal impact may induce the intensive tidal responses in both amplitude and phase shift in the wells.

Mechanisms for the water-level variations during the earthquake

Many studies have applied the tidal response of the water level to study the permeability change of well-aquifer systems (Elkhoury et al. 2006; Xue et al. 2013; Lai et al. 2014; Shi and Wang 2014; Yan et al. 2014; Shi et al. 2015; Zhang et al. 2019a, b). The most common method used for permeability change estimation from tidal analysis was demonstrated by Hsieh et al. (1987). For a homogeneous, isotropic, laterally extensive, and confined aquifer, the phase shifts between Earth tides and water level are assumed to be caused by the time required for the water

to flow into and out of the well, related to the aquifer properties. In this case, the drainage effect of groundwater level is ignored and the resulting phase shift should always be negative due to the time required for water to horizontally flow. The near zero phase shift in the D22 well sometimes show negative value, which may be interpreted by this model (Elkhoury et al. 2006). For the coseismic positive phase shifts observed in the D22 well and in the LJ well, which mean preceding water level to tidal strain, Hsieh's model no longer suffices. Roeloffs (1996) presented another model in which vertical diffusion of pore pressure to the water table can cause wave-level change in advance. Figure 7 shows that in the D22 well, the coseismic phase response changes to be positive and restores to be near zero gradually after the earthquake. Thus, these phase responses are a combination of normal phase lag caused by wellbore storage effect (aquifer confined) and coseismic phase lead caused by pore diffusion (aquifer not well confined). These observed phase responses can be considered a measurement of permeability for either horizontal or vertical fluid flows (e.g., Lai et al. 2013, 2014).

Estimation of the aquifer property changes

The coseismic phase shift of the D22 well that varies within 0° – 10° could be interpreted as a switched vertical diffusion (Shi and Wang 2016). Nevertheless, the pre-seismic and postseismic situations need to be identified. Based on Hsieh's horizontal flow model, the transmissivity T of aquifers can be estimated, which is the rate of water transmission through a unit width of aquifer under a unit hydraulic gradient as (Doan et al. 2006):

$$A = (E^2 + F^2)^{-1/2}, \quad (6)$$

$$\eta = -\tan^{-1}(F/E), \quad (7)$$

where

$$E = 1 - \frac{\omega r_c^2}{2T} [\Psi \text{Ker}(\alpha) + \Phi \text{Kei}(\alpha)] \approx 1 - \frac{\omega r_c^2}{2T} \text{Kei}(\alpha), \quad (8)$$

$$F = \frac{\omega r_c^2}{2T} [\Phi \text{Ker}(\alpha) - \Psi \text{Kei}(\alpha)] \approx \frac{\omega r_c^2}{2T} \text{Ker}(\alpha), \quad (9)$$

$$\alpha = (\omega S/T)^{-1/2} r_w, \quad (10)$$

where S is the dimensionless storage coefficient. Ker and Kei are the zero-order Kelvin functions. r_w is the radius of the well, and r_c is the inner radius of the casing. ω is the frequency of the tide. r_w and r_c can be gotten from drilling data (Fig. 2a). $\Phi = \frac{-[\text{Ker}_1(\alpha) + \text{Kei}_1(\alpha)]}{2^{1/2}\alpha[\text{Ker}_1^2(\alpha) + \text{Kei}_1^2(\alpha)]}$ and $\Psi = \frac{-[\text{Ker}_1(\alpha) - \text{Kei}_1(\alpha)]}{2^{1/2}\alpha[\text{Ker}_1^2(\alpha) + \text{Kei}_1^2(\alpha)]}$, where Ker_1 and Kei_1 are the

first-order Kelvin functions. Finally, the horizontal transmissivity T_h can be estimated in the D22 well of a confined aquifer above $10^{-4} \text{ m}^2/\text{s}$ at before and after the earthquake with low phase shift (Zhang et al. 2019b). While in a vertical pore-pressure diffusion model with positive phase shift, the pressure spreads to the free surface, the amplitude of the tide disappears (Roeloffs 1996). At the tidal frequencies, the skin length may exceed the depth of the shielding layer under where to measure the well pressure diffusion as (Shi and Wang 2016):

$$D \frac{\partial^2 p}{\partial z^2} + BK_u \frac{\partial \varepsilon}{\partial t} = \frac{\partial p}{\partial t}, \quad (11)$$

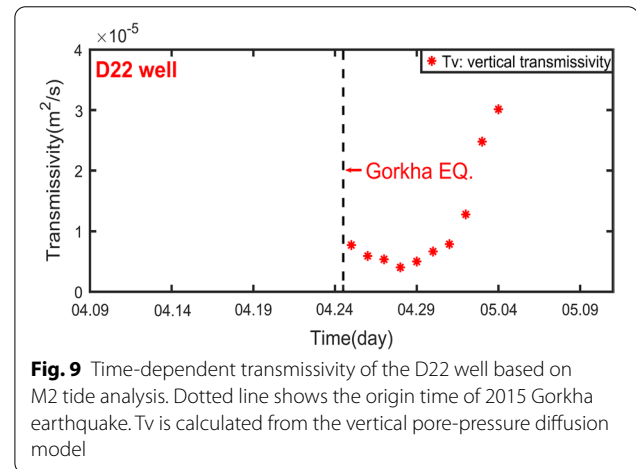
$$p(z \rightarrow \infty) = BK_u, \quad (12)$$

$$p(z = 0) = 0, \quad (13)$$

where the solution can be written as

$$p(z, \omega) = BK_u \varepsilon \left(1 - e^{-(1+i)z/\sqrt{2D/\omega}} \right), \quad (14)$$

representing the pore-pressure fluctuation at depth z . B is Skempton's coefficient. K_u is the bulk modulus of the saturated rock under undrained conditions. ε is the change in the volumetric strain. D is the hydraulic diffusivity. With the relation of vertical transmissivity $T_v = DS$, Fig. 9 shows the switched coseismic vertical transmissivity T_v in the D22 well above $3 \times 10^{-6} \text{ m}^2/\text{s}$. Considering the coherence between water level and barometric pressure is nearly 0.8 before and after the Gorkha earthquake, without distinct declinations, these results provide evidence that aquifer was confined both before and after the earthquake, which is also insensitive to changes in the horizontal transmissivity while $T_h > 10^{-4} \text{ m}^2/\text{s}$ in this well. While the coseismic turned positive phase may mean the instant seismic wave induced vertical diffusion,



which also breaks the barometric efficiency in the high-frequency band (see Fig. 5c second panel).

The phase shifts of LJ well are all positive, which may indicate leakage to the water table as the unconfined aquifer model. Figure 10 shows the coseismic enhancement of vertical transmissivity around the Gorkha earthquake. Although a hydrogeological background of layered aquifer–aquitard system may bring controversy, a surface hydrological estimation has justified the tide insensitive high horizontal transmissivity in the LJ well (Liao and Wang, 2018). Therefore, the vertical pore pressure diffusion model is applicable to interpret the coseismic response in the LJ well.

Discussion and conclusions

For the D22 well, the coseismic positive phase shift from 0° to 10° (Fig. 7) indicates vertical diffusion in a semi-confined well-aquifer system during the earthquake. We use the data from February 8 to August 7, 2015 to analyze the tidal response over a long period and identified the coseismic well water-level responses. It indicates that the well-confined aquifer before the Gorkha earthquake became semiconfined after the earthquake shaking arrival. These shifts recover at the 11th day after the earthquake plausibly related to the time window, which means a relative short-term hydrological process. Maybe, these short-term variations are captured by the small time-steps which may be sometimes ignored by the long-term tide analysis. This switch may have been caused by a reopening of vertical fractures (Liao et al. 2015), which would reseal over time (Fig. 7). Therefore, the change of aquifer type lasted 10 days and instantly recovered (Fig. 9). It is noted that the 10 days change represented the vertical reopening, and the successive meant the covariant change in clogging. The instant recovery can be interpreted as the high-frequency seismic wave induced

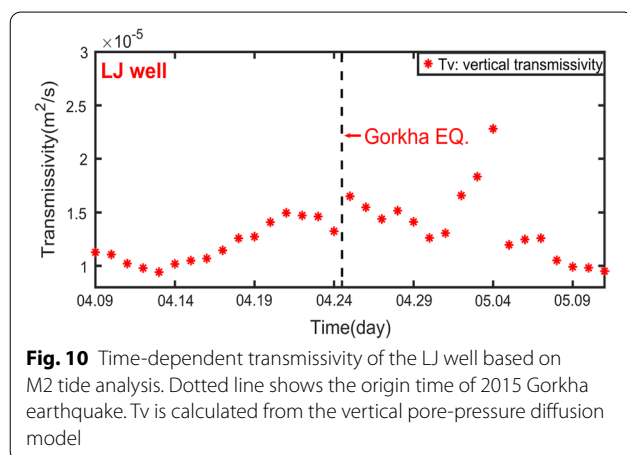
the tiny mineral particle unclogging movement in the narrow pore throat in possible vertical fractures in marl stone, hereafter minerals instantly reclogged by the vertical water diffusion after the high-frequency shaking.

For the LJ well, the coseismic enhancement in positive phase shift and decrease in amplitude ratio of the response to the M2 tide break the seasonal downward phase shift and upward amplitude ratio in 2015 (Liao and Wang 2018). Knowing the Gorkha earthquake, they can be identified as causal impact by the earthquake (Fig. 8), as the expected behaviors of unconfined aquifers. We can also infer that the Gorkha earthquake had only short-time influence on the continuously seasonal vertical leakage at the LJ well. The LJ well remained well unconfined during the earthquake. By the continuous monitor of the vertical transmissivity (T_v), the distinct enhancement 8th day after the earthquake can last 3 days (see Fig. 10). The total recovery to the preseismic state also happened at 11th day after the earthquake. The enhancement of the vertical transmissivity following the Gorkha earthquake may be caused by the further unclogging of preexisting fractures aligned with the local groundwater flow perturbation after the shaking of seismic waves, which is also followed by an instant recovery to the common state.

Many studies have documented the earthquake-induced water permeability switching and enhancement in the near field (epicentral distance < 1 rupture length) and intermediate field (Rojstaczer et al. 1995; Manga and Rowland 2009; Manga et al. 2012; Shi and Wang 2014, 2016; Wang and Manga 2015; Wang et al. 2018). The postseismic healing or reclogging of fractures permeability will restore permeability (Xue et al. 2013; Shi and Wang 2015). The epicentral distances for the Gorkha earthquake of the two wells are similar in far field (several times rupture length ~ 1500 km, see Table 1). Using the empirical seismic energy estimation as (Wang 2007):

$$\log(r) = 0.48M - 0.33\log(e) - 1.4, \quad (15)$$

where r is the actual epicentral distance in kilometers, M is the earthquake magnitude, and e is the seismic energy density (in Jm^{-3}). The seismic energy density at the D22 well was $3.4 \times 10^{-3} \text{ Jm}^{-3}$, while at the LJ well was $2.8 \times 10^{-3} \text{ Jm}^{-3}$, using this relation derived in southern California, which were not consistent to the peak ground velocity (PGV) estimated from the seismograms (Fig. 3). The PGV at the LJ well was two orders of magnitude greater. However, the epicenter distance of it is longer (1530.9 km), and coseismic water-level response magnitude and duration was shorter (Fig. 1 and Table 1), which may induce the corresponding response in water level. We also calculated the static strain caused by the Gorkha earthquake based on the Okada model (Lin and Stein 2004; Toda et al. 2005; Zhang et al. 2015), which



turns out to be about magnitude of 10^{-12} (positive for dilatation). It is too small to cause water-level rise, indicating that the effects of static strain on the coseismic water-level change in the far field are negligible. The water-level changes may only be caused by the dynamic strain induced by seismic waves. We infer that the local site amplification effect may make these abnormal seismic responses, which may further differ the hydrological responses under the hydrogeological backgrounds (Liao and Wang 2018). The main aquifer lithology of the LJ well is dolomitic limestone that is aquitard, but more suitable for fracture development than the marl stone in the D22 well (e.g., Mavko et al. 2003). Under the rough estimation of seismic energy at the two wells, about 10^{-3} Jm^{-3} is capable of triggering different hydrological responses (Wang and Manga 2015). Therefore, it is reasonable to deduce whether the vertical fracture becomes active and totally heals at these two far-field wells can be referred to the high-frequency seismic waves. Aquifer-type change may occur at the D22 well. The unclogging and reclogging may represent the tiny mineral colloidal particle movement and accumulation in narrow pore throat induced by the less seismic energy during the earthquake (see Fig. 3).

Comparing Figs. 9 and 10, we can see instant healing process during about 10-day period after the Gorkha earthquake. At the D22 well, the aquifer-type change of the switched vertical transmissivity changed from $0 \text{ m}^2/\text{s}$ to around $1 \times 10^{-5} \text{ m}^2/\text{s}$ after the earthquake and decreased further to $0 \text{ m}^2/\text{s}$ of total vertical healing. The distinct vertical transmissivity changes induced by the earthquake in the LJ well lasted 10 days. The persistent vertical transmissivity changed from about $1.3 \times 10^{-5} \text{ m}^2/\text{s}$ to $1.7 \times 10^{-5} \text{ m}^2/\text{s}$, but returned to $1.2 \times 10^{-5} \text{ m}^2/\text{s}$ as the preseismic stage. These resealing may have been caused by the partial blocking of preexisting fractures induced by the Gorkha earthquake, indicating that the local hydrogeological conditions (e.g., permeability, aquifer lithology, and fracture aperture) are important to the recovery process.

The coherence of water level and seismic wave indicated that the coseismic hydrogeological responses were induced by high-frequency ($f > 8 \text{ cpd}$) ground oscillations with the high dynamic seismic energy. The recoveries only lasted 10 days which also means high-frequency impact did not make persistent change in aquifer system, different from that as reported after the 2011 Tohoku earthquake (see Zhang et al. 2019b). With the observations of short time-step, we can discover this short-term change. The wells are distant (about 1500 km) to the epicenter, and they are all affected by the Tibet plateau geological evolution. The various far-field hydrogeological responses, especially a coseismic aquifer-type change to semiconfined, may be

considered as a significant factor in earthquake fluid monitoring in the seismic active area to great earthquakes.

Supplementary Information

The online version contains supplementary material available at <https://doi.org/10.1186/s40623-021-01441-0>.

Additional file 1: **Text S1.** Two 1-hour sampling 60-day synthetic data without and with an impulse. **Text S2.** Phase-shift estimation using the Baytap-G software. **Figure S1.** The 1-hour sampling 60-day synthetic data with a phase change in the M2 period on the 31st day. The red dotted line represents the time when the phase change occurs. **Figure S2.** The 1-hour sampling 60-day synthetic data with a phase change in the M2 period and an impulse on the 31st day. The red dotted line represents the time when the phase change and the impulse occur. **Figure S3.** The phase shift with error bars of the 60-day synthetic data without (a) and with the impulse (b) to the M2 tide using the Baytap-G software with different time windows. The highlighted error bars indicate the error of the tidal analysis. The black dotted lines represent the time when the phase change or the impulse occurs. The vertically downward red arrows point the last time windows that contain the phase change. **Figure S4.** The phase shift with error bars of the 60-day synthetic data without (a) and with the impulse (b) to the S2 tide using the Baytap-G software with different time windows. The highlighted error bars indicate the error of the tidal analysis. The black dotted lines represent the time when the phase change or the impulse occurs.

Acknowledgements

We thank the China Earthquake Administration for providing the data used in this study.

Authors' contributions

XH and YZ carried out most of geologic investigation, data collection, and data pre-treatment. XH finished the calculation and analysis of coherence and tidal responses and calculated the transmissivities. YZ finished the coseismic hydrological analysis. XH and YZ conceived and coordinated the study, drafted and approved the manuscript. All authors read and approved the final manuscript.

Funding

This research is financially supported by the National Natural Science Foundation of China (NSFC), under Grant No. 41774119, the special Fundamental Research Funds for the Central Universities (2042017kf0228) and Wuhan University Experiment Technology Project Funding (WHU-2019-SYJS-12).

Availability of data and materials

The data used in this study can be applied from the National Earthquake Data Center of the China Earthquake Administration (<http://earthquake.cn/>).

Declaration

Competing interests

The authors declare that they have no competing interests.

Author details

¹School of Geodesy and Geomatics, Wuhan University, Wuhan 430079, China.

²Key Laboratory of Geospace Environment and Geodesy, Ministry of Education, Wuhan 430079, China.

Received: 11 January 2021 Accepted: 18 May 2021

Published online: 31 May 2021

References

- Avouac JP, Meng LS, Wei SJ, Wang T, Ampuero JP (2015) Lower edge of locked Main Himalayan Thrust unzipped by the 2015 Gorkha earthquake. *Nat Geosci* 8(9):708–711. <https://doi.org/10.1038/Ngeo2518>
- Brodsky EE, Roeloffs E, Woodcock D, Gall I, Manga M (2003) A mechanism for sustained groundwater pressure changes induced by distant earthquakes. *J Geophys Res* 108(B8):503–518. <https://doi.org/10.1029/2002jB002321>
- Claesson L, Skelton A, Graham C, Dietl C, Mörth M, Torssander P, Kockum I (2004) Hydrogeochemical changes before and after a major earthquake. *Geology* 32(8):641–644. <https://doi.org/10.1130/G20542.1>
- Claesson L, Skelton A, Graham C, Mörth CM (2007) The timescale and mechanisms of fault sealing and water-rock interaction after an earthquake. *Geofluids* 7(4):427–440. <https://doi.org/10.1111/j.1468-8123.2007.00197.x>
- Cooper HH, Bredehoeft JD, Papadopoulos IS, Bennett RR (1965) The response of well-aquifer systems to seismic waves. *J Geophys Res* 70(16):3915–3926. <https://doi.org/10.1029/JZ070i016p03915>
- Deng QD, Zhang PZ, Ran YK (2006) Distribution of active faults in China (1:4000000). Science Press, Beijing
- Doan ML, Brodsky EE, Prioul R, Signer C (2006) Tidal analysis of borehole pressure—a tutorial. Schlumberger Research Report
- Elkhoury JE, Brodsky EE, Agnew DC (2006) Seismic waves increase permeability. *Nature* 441(7097):1135–1138. <https://doi.org/10.1038/nature04798>
- Elliott JR, Jolivet R, Gonzalez PJ, Avouac JP, Hollingsworth J, Searle MP, Stevens VL (2016) Himalayan megathrust geometry and relation to topography revealed by the Gorkha earthquake. *Nat Geosci* 9(2):174–180. <https://doi.org/10.1038/Ngeo2623>
- Feng WP, Zhang JF, Tian YF, Gong LX (2004) Analysis of the characteristic about the Honghe active fault zone based on the ETM plus remote sensing images. *Int Geosci Remote Sensing Symp* 5:2985–2987
- Hsieh PA, Bredehoeft JD, Farr JM (1987) Determination of aquifer transmissivity from earth tide analysis. *Water Resour Res* 23(10):1824–1832. <https://doi.org/10.1029/WR023i010p01824>
- Jónsson S, Segall P, Pedersen R, Björnsson G (2003) Post-earthquake ground movements correlated to pore-pressure transients. *Nature* 424(6945):179–183. <https://doi.org/10.1038/nature01776>
- Kagabu M, Ide K, Hosono T, Nakagawa K, Shimada J (2020) Describing coseismic groundwater level rise using tank model in volcanic aquifers, Kumamoto, southern Japan. *J Hydrol* 582:124464. <https://doi.org/10.1016/j.jhydrol.2019.124464>
- Lai GJ, Ge HK, Wang WL (2013) Transfer functions of the well-aquifer systems response to atmospheric loading and Earth tide from low to high-frequency band. *J Geophys Res* 118(5):1904–1924. <https://doi.org/10.1002/jgrb.50165>
- Lai GJ, Ge HK, Xue L, Brodsky EE, Huang FQ, Wang WL (2014) Tidal response variation and recovery following the Wenchuan earthquake from water level data of multiple wells in the nearfield. *Tectonophysics* 619:115–122. <https://doi.org/10.1016/j.tecto.2013.08.039>
- Liao X, Wang CY (2018) Seasonal permeability change of the shallow crust inferred from deep well monitoring. *Geophys Res Lett* 45(20):11130–11136. <https://doi.org/10.1029/2018gl080161>
- Liao X, Wang CY, Liu CP (2015) Disruption of groundwater systems by earthquakes. *Geophys Res Lett* 42(22):9758–9763. <https://doi.org/10.1002/2015gl066394>
- Lin J, Stein RS (2004) Stress triggering in thrust and subduction earthquakes and stress interaction between the southern San Andreas and nearby thrust and strike-slip faults. *J Geophys Res* 109(B2):B02303. <https://doi.org/10.1029/2003jb002607>
- Ma Y (2016) Earthquake-related temperature changes in two neighboring hot springs at Xiangcheng. *China Geofluids* 16(3):434–439. <https://doi.org/10.1111/gfl.12161>
- Ma YC, Huang FQ (2017) Coseismic water level changes induced by two distant earthquakes in multiple wells of the Chinese mainland. *Tectonophysics* 694:57–68. <https://doi.org/10.1016/j.tecto.2016.11.040>
- Manga M (2001) Origin of postseismic streamflow changes inferred from baseflow recession and magnitude-distance relations. *Geophys Res Lett* 28(10):2133–2136. <https://doi.org/10.1029/2000gl012481>
- Manga M, Rowland JC (2009) Response of Alum Rock springs to the October 30, 2007 Alum Rock earthquake and implications for the origin of increased discharge after earthquakes. *Geofluids* 9(3):237–250. <https://doi.org/10.1111/j.1468-8123.2009.00250.x>
- Manga M, Brodsky EE, Boone M (2003) Response of streamflow to multiple earthquakes. *Geophys Res Lett* 30(5):1214. <https://doi.org/10.1029/2002g1016618>
- Manga M, Beresnev I, Brodsky EE, Elkhoury JE, Elsworth D, Ingebritsen SE, Mays DC, Wang CY (2012) Changes in permeability caused by transient stresses: field observations, experiments, and mechanisms. *Rev Geophys* 50(2):81–88. <https://doi.org/10.1029/2011rg000382>
- Mavko G, Mukerji T, Dvorkin J (2003) The rock physics handbook. Cambridge University Press, Cambridge
- Menke W, Menke J (2016) Environmental data analysis with Matlab, 2nd edn. Academic Press, New York
- Mogi K, Mochizuki H, Kurokawa Y (1989) Temperature-changes in an Artesian Spring at Usami in the Izu Peninsula (Japan) and their relation to earthquakes. *Tectonophysics* 159(1–2):95–108. [https://doi.org/10.1016/0040-1951\(89\)90172-8](https://doi.org/10.1016/0040-1951(89)90172-8)
- Muir-wood R, King GCP (1993) Hydrological signatures of earthquake strain. *J Geophys Res* 98(B12):22035–22068. <https://doi.org/10.1029/93jb02219>
- Roeloffs E (1996) Poroelastic techniques in the study of earthquake-related hydrologic phenomena. *Adv Geophys* 37:135–195. [https://doi.org/10.1016/S0065-2687\(08\)60270-8](https://doi.org/10.1016/S0065-2687(08)60270-8)
- Roeloffs EA (1998) Persistent water level changes in a well near Parkfield, California, due to local and distant earthquakes. *J Geophys Res* 103(B1):869–889. <https://doi.org/10.1029/97jb02335>
- Rojstaczer S, Agnew DC (1989) The influence of formation material properties on the response of water levels in wells to earth tides and atmospheric loading. *J Geophys Res* 94(B9):12403–12411. <https://doi.org/10.1029/JB094iB09p12403>
- Rojstaczer S, Wolf S, Michel R (1995) Permeability enhancement in the shallow crust as a cause of earthquake-induced hydrological changes. *Nature* 373(6511):237–239. <https://doi.org/10.1038/373237a0>
- Shi ZM, Wang GC (2014) Hydrological response to multiple large distant earthquakes in the Mile well. *China J Geophys Res* 119(11):2448–2459. <https://doi.org/10.1002/2014jf003184>
- Shi ZM, Wang GC (2015) Sustained groundwater level changes and permeability variation in a fault zone following the 12 May 2008, Mw 7.9 Wenchuan earthquake. *Hydrol Process* 29(12):2659–2667. <https://doi.org/10.1002/hyp.10387>
- Shi ZM, Wang GC (2016) Aquifers switched from confined to semiconfined by earthquakes. *Geophys Res Lett* 43(21):11166–11172. <https://doi.org/10.1002/2016gl070937>
- Shi Y, Cao J, Ma L, Yin B (2007) Tele-seismic coseismic well temperature changes and their interpretation. *Acta Seismol Sin* 29(3):280–289. <https://doi.org/10.1007/s11589-007-0280-z>
- Shi ZM, Wang GC, Liu CL, Mei JC, Wang JW, Fang HN (2013) Coseismic response of groundwater level in the three gorges well network and its relationship to aquifer parameters. *Chinese Sci Bull* 58(25):3080–3087. <https://doi.org/10.1007/s11434-013-5910-3>
- Shi ZM, Wang GC, Manga M, Wang CY (2015) Mechanism of co-seismic water level change following four great earthquakes—insights from co-seismic responses throughout the Chinese mainland. *Earth Planet Sc Lett* 430:66–74. <https://doi.org/10.1016/j.epsl.2015.08.012>
- Sibson RH, Rowland JV (2003) Stress, fluid pressure and structural permeability in seismogenic crust, North Island. *New Zealand Geophys J Int* 154(2):584–594. <https://doi.org/10.1046/j.1365-246X.2003.01965.x>
- Skelton A, Andrén M, Kristmannsdóttir H, Stockmann G, Mörth CM, Sveinbjörnsdóttir Á, Jónsson S, Sturkell E, Guðrúnardóttir HR, Hjartarson H, Siegmund H, Kockum I (2014) Changes in groundwater chemistry before two consecutive earthquakes in Iceland. *Nat Geosci* 7(10):752–756. <https://doi.org/10.1038/Ngeo2250>
- Tamura Y, Sato T, Ooe M, Ishiguro M (1991) A procedure for tidal analysis with a Bayesian information criterion. *Geophys J Int* 104(3):507–516. <https://doi.org/10.1111/j.1365-246X.1991.tb05697.x>
- Toda S, Stein RS, Richards-Dinger K, Bozkurt SB (2005) Forecasting the evolution of seismicity in southern California: animations built on earthquake stress transfer. *J Geophys Res* 110(B5):B05S16. <https://doi.org/10.1029/2004jb003415>
- Wang CY (2007) Liquefaction beyond the near field. *Seismol Res Lett* 78(5):512–517. <https://doi.org/10.1785/gssrl.78.5.512>
- Wang CY, Manga M (2015) New streams and springs after the 2014 Mw6.0 South Napa earthquake. *Nat Commun* 6:7597. <https://doi.org/10.1038/ncomms8597>

- Wang CY, Wang CH, Manga M (2004b) Coseismic release of water from mountains: evidence from the 1999 (M-W=7.5) Chi-Chi, Taiwan, earthquake. *Geology* 32(9):769–772. <https://doi.org/10.1130/G20753.1>
- Wang CY, Manga M, Dreger D, Wong A (2004a) Streamflow increase due to rupturing of hydrothermal reservoirs: evidence from the 2003 San Simeon, California. *Earthquake Geophys Res Lett* 31(10):L10502. <https://doi.org/10.1029/2004gl020124>
- Wang CY, Wang LP, Manga M, Wang CH, Chen CH (2013) Basin-scale transport of heat and fluid induced by earthquakes. *Geophys Res Lett* 40(15):3893–3897. <https://doi.org/10.1002/grl.50738>
- Wang CY, Doan ML, Xue L, Barbour AJ (2018) Tidal response of groundwater in a leaky aquifer-application to Oklahoma. *Water Resour Res* 54(10):8019–8033. <https://doi.org/10.1029/2018wr022793>
- Wang CY, Zhu AY, Liao X, Manga M, Wang LP (2019) Capillary effects on groundwater response to earth tides. *Water Resour Res* 55(8):6886–6895. <https://doi.org/10.1029/2019wr025166>
- Xue L, Li HB, Brodsky EE, Xu ZQ, Kano Y, Wang H, Mori JJ, Si JL, Pei JL, Zhang W, Yang G, Sun ZM, Huang Y (2013) Continuous permeability measurements record healing inside the Wenchuan Earthquake Fault Zone. *Science* 340(6140):1555–1559. <https://doi.org/10.1126/science.1237237>
- Yan R, Woith H, Wang RJ (2014) Groundwater level changes induced by the 2011 Tohoku earthquake in China mainland. *Geophys J Int* 199(1):533–548. <https://doi.org/10.1093/gji/ggu19>
- Zeng XP, Lin YF, Chen WS, Bai ZQ, Liu JY, Chen CH (2015) Multiple seismo-anomalies associated with the M6.1 Ludian earthquake on August 3, 2014. *J Asian Earth Sci* 114:352–361. <https://doi.org/10.1016/j.jseas.2015.04.0276>
- Zhang Y, Fu LY, Huang FQ, Chen XZ (2015) Coseismic water-level changes in a well induced by teleseismic waves from three large earthquakes. *Tectonophysics* 651:232–241. <https://doi.org/10.1016/j.tecto.2015.02.027>
- Zhang Y, Fu LY, Ma YC, Hu JH (2016) Different hydraulic responses to the 2008 Wenchuan and 2011 Tohoku earthquakes in two adjacent far-field wells: the effect of shales on aquifer lithology. *Earth Planets Space* 68:178. <https://doi.org/10.1186/s40623-016-0555-5>
- Zhang Y, Wang CY, Fu LY, Zhao B, Ma YC (2019b) Unexpected far-field hydrological response to a great earthquake. *Earth Planet Sc Lett* 519:202–212. <https://doi.org/10.1016/j.epsl.2019.05.007>
- Zhang H, Shi Z, Wang G, Sun X, Yan R, Liu C (2019a) Large earthquake reshapes the groundwater flow system: insight from the water-level response to earth tides and atmospheric pressure in a deep well. *Water Resour Res* 55(5):4207–4219. <https://doi.org/10.1029/2018wr024608>

Publisher's Note

Springer Nature remains neutral with regard to jurisdictional claims in published maps and institutional affiliations.

Submit your manuscript to a SpringerOpen[®] journal and benefit from:

- Convenient online submission
- Rigorous peer review
- Open access: articles freely available online
- High visibility within the field
- Retaining the copyright to your article

Submit your next manuscript at ► [springeropen.com](https://www.springeropen.com)